CrystEngComm

PAPER

View Article Online
View Journal | View Issue

Cite this: *CrystEngComm*, 2014, **16**, 2950

One-pot solvothermal synthesis of a well-ordered layered sodium aluminoalcoholate complex: a useful precursor for the preparation of porous Al_2O_3 particles†

Xiansen Li,*[a] Vladimir K. Michaelis,[bc] Ta-Chung Ong,[bc] Stacey J. Smith,[b] Ian McKay,[a] Peter Müller,[b] Robert G. Griffin[bc] and Evelyn N. Wang*[a]

Received 23rd December 2013,
Accepted 20th January 2014

DOI: 10.1039/c3ce42616e

www.rsc.org/crystengcomm

One-pot solvothermal synthesis of a robust tetranuclear sodium hexakis(glycolato)tris(methanolato)aluminate complex $Na_3[Al_4(OCH_3)_3(OCH_2CH_2O)_6]$ *via* a modified yet rigorous base-catalyzed transesterification mechanism is presented here. Single crystal X-ray diffraction (SCXRD) studies indicate that this unique Al complex contains three pentacoordinate Al^{3+} ions, each bound to two bidentate ethylene glycolate chelators and one monodentate methanolate ligand. The remaining fourth Al^{3+} ion is octahedrally coordinated to one oxygen atom from each of the six surrounding glycolate chelators, effectively stitching the three pentacoordinate Al moieties together into a novel tetranuclear Al complex. This aluminate complex is periodically self-assembled into well-ordered layers normal to the [110] axis with the intra-/inter-layer bonding involving extensive ionic bonds from the three charge-counterbalancing Na^+ cations rather than the more typical hydrogen bonding interactions as a result of fewer free hydroxyl groups present in its structure. It can also serve as a valuable precursor toward the facile synthesis of high-surface-area alumina powders using a very efficient rapid pyrolysis technique.

Introduction

Layered materials containing coordinatively unsaturated bonding sites such as 5-coordinate Al ($^{[5]}$Al) species are of topical interest because they promise improved performance for lithium-/sodium-ion batteries,[1] adsorbent,[2] and catalyst[3] applications. Among these, intercalated layered materials have attracted considerable attention due to their tunable pore size and versatile guest species such as Li^+ and Na^+ cations for increased adsorption capacity and selectivity. They are also important precursors towards preparing nanoscale porous lamellas,[4] nanotubes,[5] and composite materials.[6]

Solvothermal synthesis exhibits a significant advantage over the conventional hydrothermal technique in cases where either moisture sensitive reagents or potential occurrence of insoluble metal hydroxide side-reactions is inevitably involved in the preparation. Solvothermal synthesis involving polyols (*e.g.*, 1,2-diols) as the solvent has so far been moderately explored for the preparation of novel zeolites,[7] silicopolyolate containing interesting $^{[5]}$Si species,[8] and an aluminoglycolate analogue containing fascinating $^{[5]}$Al geometry.[9] For example, Gainsford *et al.* reported a trinuclear $[Al_3(OCH_2CH_2O)_5(OCH_2CH_2OH)_2]^{3-}$ anion and several concomitant by-products prepared *via* direct reaction between alumina and NaOH in considerably excessive ethylene glycol (EG) solvent by slowly distilling off both EG and any liberated water from the reaction during the synthesis period until it reached the pseudo-saturation state, followed by a recrystallization step.[9d]

Although the $^{[4]}$Al and $^{[6]}$Al species in zeolites, clays, minerals, *etc.* have been well studied,[10] relatively few $^{[5]}$Al species have been reported in alkoxide-based crystalline solids to date.[9,11] Consequently, much less is known about their physicochemical properties, *e.g.*, the chemical-shift "fingerprint" region of ^{27}Al magic angle spinning nuclear magnetic resonance (MAS NMR) spectra for these unique $^{[5]}$Al environments. The study of this unique structure is expected

[a] *Department of Mechanical Engineering, Massachusetts Institute of Technology, Cambridge, Massachusetts 02139, USA. E-mail: xsli@mit.edu, enwang@mit.edu; Tel: +1 617 324 3311*
[b] *Department of Chemistry, Massachusetts Institute of Technology, Cambridge, Massachusetts 02139, USA*
[c] *Francis Bitter Magnet Laboratory, Massachusetts Institute of Technology, Cambridge, Massachusetts 02139, USA*

† Electronic supplementary information (ESI) available: Representations of the methanol occupancy and positional disorders of some atoms. Packing structures along the *c* and [$\bar{1}$10] axes. CIF file for the aluminate complex. CCDC 955650. For ESI and crystallographic data in CIF or other electronic format see DOI: 10.1039/c3ce42616e

to extend the horizons of such existing systems. We herein report the asymmetric tetranuclear Al complex with three $^{[5]}$Al species, which was achieved using a modified transesterification synthetic strategy. In addition, we demonstrated the possibilities and benefits of using this layered Al complex as a valuable precursor for efficient preparation of high value-added nanoporous Al_2O_3 powders that are of great relevance both academically and industrially as catalysts, catalyst supports, adsorbents, refractory ceramics, and active feedstocks.

Results and discussion

We present a novel solvothermal preparative method *via* a modified base-catalyzed transesterification mechanism, which has been quite scarcely explored for hybrid inorganic/organic materials preparations,[12] for the synthesis of a layered aluminoalcoholate complex in the presence of methanol as solvent rather than the more commonly used EG solvent. In the course of the solvothermal reaction, the effective deprotonation from the slightly excessive EG reactant is initially implemented by the action of an aliquot of a strong base catalyst of sodium methoxide to initiate the S_N2 nucleophilic substitution reaction, leading to the formation of bidentate ethylene glycolate chelators. These incoming chelators thus formed then compete with three aliquots of sodium methanolate for nucleophilic attack of the Al electrophiles, causing the concurrent departure of $CH_3CH_2O^-$ anions (Scheme 1). Due to the chelate nature of the bidentate glycolate ligand, Al electrophiles as ligand acceptors possess a coordinative preference for glycolate ligands over monodentate methanolate ones, thus affording a unique mixed $^{[5]}$Al/$^{[6]}$Al complex at a methanolate/glycolate ratio of 1 : 2 in the final empirical formula. The complexing power with central Al^{3+} cations decreases in the following order: $[OCH_2CH_2O]^{2-} > CH_3O^- > CH_3CH_2O^-$. The $NaOCH_3$ catalyst is ultimately regenerated by reacting the resultant $NaOCH_2CH_3$ with the MeOH formed in the first deprotonation step. It is worth noting that sodium methoxide in slight excess was employed as both the transesterifying base catalyst and one of the reactants. The newly formulated approach is unusual in that only single-step synthesis is utilized without any laborious cycles of fractional-/vacuum-distillations required by previous researchers such as Gainsford *et al.*[9d] More importantly, this approach is versatile since it only implicates alkali metal alkoxide base-catalyzed alcoholysis but without any intervention of detectable alkaline (OH^-) hydrolysis side-reactions.

In the solvothermal synthesis, the conventional organic transesterification reaction was adapted such that the routine carboxylic acid ester was replaced with a pseudo-covalent metal/non-metal alkoxide ester, as exemplified specifically in Scheme 1. This reversible S_N2 nucleophilic substitution reaction involving a competitive ligand-exchange step is expected to be an efficient way to rationally tailor the relative contributions between the nucleation and crystal growth events, thus favoring the efficient large single crystal production. The alcohol-selective rule manifests the possibility of crystal composition tailoring by judiciously choosing different monohydroxy alcohols and polyols. Solvothermal crystallization at 181 °C for 5 days resulted in an end product with an actual chemical formula of $Na_3[Al_4(OCH_3)_3(OCH_2CH_2O)_6]$. It is anticipated that the coupled high synthetic temperature and high autogenous vapor pressure[13] applied in the synthesis enable the formation of the largest tetranuclear Al complex of its kind ever reported in the literature. The multinuclear nature of this Al complex may explain its insolubility in MeOH, only slight solubility in water and EG, and enhanced stability against both hydrolysis and alcoholysis. This synthetic strategy is universal as long as the large electronegative metal/non-metal (*e.g.*, Si and B) can be prepared in the form of corresponding alkoxides and is restricted neither by the insolubility of metal oxide/hydroxide in alkaline solutions nor by the potential formation of insoluble metal hydroxide impurities *in situ* during synthesis, as encountered by other researchers.[14] Moreover, the reactants are not only limited to alkoxide esters but also include a variety of organic-soluble salts (*e.g.*, chlorides), organometallics and labile metal complexes over the corresponding metalloalcoholate ones, although the latter category of reactions cannot be strictly classified as transesterification reactions.

$$4Al(OC_2H_5)_3\ \text{(ester)} + 6EG\ \text{(alcohol)} + 3NaOCH_3 \xrightleftharpoons[\Delta,\ MeOH\ (solv.)]{NaOCH_3\ (cat.)} Na_3[Al_4(OCH_3)_3(OCH_2CH_2O)_6]\ \text{(new ester)} + 12EtOH\ \text{(new alcohol)}$$

Scheme 1 Proposed reaction pathway to the target product $Na_3[Al_4(OCH_3)_3(OCH_2CH_2O)_6]$ starting with aluminium alkoxide, EG and sodium methoxide by a modified transesterification mechanism.

The details of the crystal structure and its structural refinement are listed in Table 1. The Al compound crystallizes in the monoclinic crystal system and space group $P2_1/c$.

As determined by SCXRD, the asymmetric unit (AU) in the crystal structure contains one sodium hexakis(glycolato)tris(methanolato)aluminate complex $Na_3[Al_4(OCH_3)_3(OCH_2CH_2O)_6]$ (Fig. 1). Three of the four Al^{3+} ions reside in considerably distorted $^{[5]}$Al environments of rectangular pyramidal geometries rather than the more expected trigonal bipyramids by inspecting the O–Al–O bond angles. The remaining fourth Al^{3+} ion in the complex is octahedrally coordinated to one oxygen atom from each of the six glycolate units in the AU, effectively tethering together the three surrounding $^{[5]}$Al monomers into a tetranuclear configuration (*i.e.*, secondary building unit (BU)) by sharing the basal edges of AlO_5 pentahedra.

The interatomic distances selectively listed in Fig. 1 caption signify a range of Al–O bond strengths for various ligands and Al species. Bonding behaviors in $^{[5]}$Al moieties are contracted Al–O bonds to the monodentate methanolate oxygens [Al–O, 1.7539(14)–1.7784(13) Å] compared with bidentate glycolate Al–O bonds [1.7836(14)–1.9122(13) Å]. The shorter Al–O bonds observed for the glycolates invariably involve O atoms with strong Coulombic Na^+–O interactions. In contrast, the Al–O bond length in the $^{[6]}$Al moiety ranges from 1.8714(13) [Al(1)–O(1)] to 1.9014(13) Å [Al(1)–O(8)]. By comparison, an average Al–O bond length in zeolites is 1.74 Å,

Table 1 Crystallographic data and structural refinement for the Al complex

Parameter	Data
CCDC no.	955650
Empirical formula	$C_{15}H_{33}Al_4Na_3O_{15}{\cdot}0.1CH_4O$
F.W.	633.35
Temperature	100(2) K
Wavelength	0.71073 Å
Crystal system	Monoclinic
Space group	$P2_1/c$
Unit cell dimensions	a = 11.2481(12) Å; α = 90°
	b = 13.1877(14) Å; β = 105.738(2)°
	c = 18.235(2) Å; γ = 90°
Volume	2603.5(5) Å^3
Z	4
Density (calculated)	1.616 Mg m^{-3}
Absorption coefficient	0.299 mm^{-1}
F(000)	1319
Crystal size	0.11 × 0.04 × 0.01 mm^3
θ collection range	1.88 to 30.99°
Index ranges	$-16 \le h \le 15$, $-19 \le k \le 18$, $-26 \le l \le 26$
Reflections collected	67 765
Independent reflections	8270 [R_{int} = 0.0539]
Completeness to θ = 30.99°	99.7%
Absorption correction	Semi-empirical from equivalents
Max. and min. transmission	0.9970 and 0.9678
Refinement method	Full-matrix least-squares on F^2
Data/restraints/parameters	8270/459/395
Goodness-of-fit on F^2	1.046
Final R indices [$I > 2\sigma(I)$]	R_1 = 0.0405, wR_2 = 0.0994
R indices (all data)	R_1 = 0.0633, wR_2 = 0.1110
Largest diff. peak and hole	0.521 and −0.438 e Å^{-3}

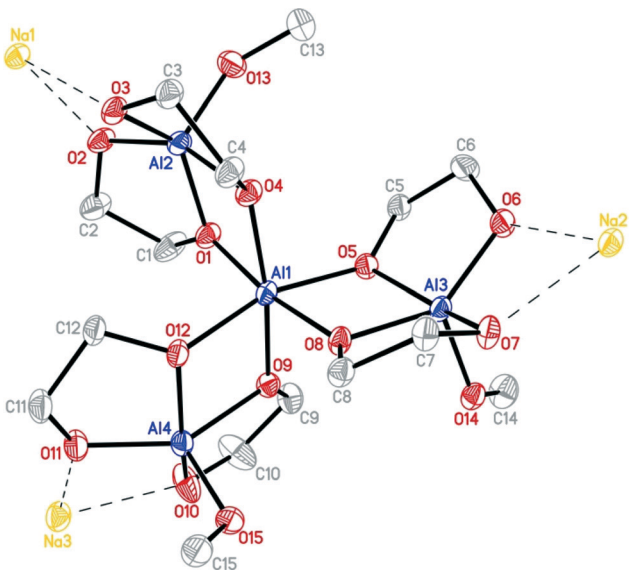

Fig. 1 Asymmetric-unit structure of the aluminate complex $Na_3[Al_4(OCH_3)_3(OCH_2CH_2O)_6]$ comprising three $^{[5]}$Al moieties stitched together by a fourth $^{[6]}$Al. Hydrogen atoms are omitted for clarity, and thermal ellipsoids are set to 50% probability. Selected interatomic bond distances (Å) and bond angles (°): Al(2)–O(13): 1.7539(14), Al(3)–O(14): 1.7784(13), Al(4)–O(15): 1.7661(14), Al(4)–O(11): 1.7836(14), Al(4)–O(12): 1.9122(13), Al(1)–O(1): 1.8714(13), and Al(1)–O(8): 1.9014(13); Al(1)–O(12)–Al(4): 101.24(6) and Al(1)–O(9)–Al(4): 103.42(6).

which is slightly shorter than the shortest Al–O distance in this aluminoalcoholate anion. Additionally, the average O–Al–O bond angle (109.5°, in close proximity to the tetrahedral value of 109.4°) in zeolites[15] lies intermediate among all of the O–Al–O bond angles in this Al complex due to the severe structural distortion of the latter Al polyhedra. On the other hand, the Al–O–Al linkage is generally forbidden in aluminosilicate zeolitic frameworks according to the Loewenstein rule[16] obeying Pauling's electrostatic valence principle but with several exceptions for naturally occurring zeolite minerals (*e.g.*, analcime,[17] stilbite[18] and lazurite[19]). Zeolites have a representative T–O–T [T (tetrahedral) = Al or Si] bond angle of 141°[15] which is much larger than Al(1)–O–Al counterparts varying in a much narrower range from 101.24(6) to 103.42(6)°. The magnitude of the Coulombic electrostatic repulsive interaction ($^{[4]}$Al$^-$–O–$^{[4]}$Al$^-$ electrostatic repulsion between Al anions in zeolites *vs.* $^{[5]}$Al$^{0.67-}$–O–$^{[6]}$Al$^-$ one in the latter) can cause this big angular difference and is what enables the existence of Al–O–Al linkages in the Al complex as opposed to synthetic zeolites.

Corroborating the SCXRD studies, the ^{27}Al MAS NMR spectrum (Fig. 2) reveals two highly crystalline Al sites with a 1 : 3 ratio. The simulated ^{27}Al NMR parameters for Site 1 (δ_{iso} = 6 ppm and a quadrupolar coupling constant of C_Q < 2 MHz) are consistent with the octahedral environment determined by SCXRD. The second site therefore corresponds to the $^{[5]}$Al nuclei exhibiting a unique $\delta_{iso} \approx 62$ ppm, a moderate C_Q = 5.5 MHz and an asymmetry parameter, η = 0.95. The larger quadrupolar coupling for Site 2 causes a second order broadening which spans 3 kHz at the base. The larger C_Q and η are due to the greater distortion/asymmetry of the $^{[5]}$Al sites relative to the $^{[6]}$Al one. An unusual chemical shift is observed for the $^{[5]}$Al environment as other well-characterized Al-containing oxides are generally located between 20 and 50 ppm.[10]

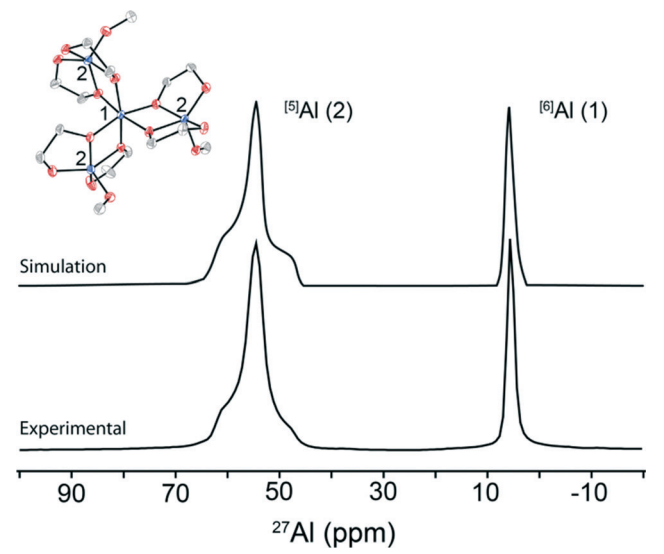

Fig. 2 ^{27}Al MAS NMR spectrum acquired at 16.4 T (experimental) and corresponding simulation of two distinct aluminium coordination environments, *i.e.*, 5-coordinate ($^{[5]}$Al) and 6-coordinate ($^{[6]}$Al).

The unique chemical shift is believed to arise from the very unique local structure of the asymmetric unit (Fig. 1) and large Columbic interactive forces (*vide supra*) whereby one $^{[6]}$Al is surrounded by three $^{[5]}$Al species creating a localized pseudo-three-fold symmetry. Each $^{[5]}$Al species is further capped by two bidentate glycolate ligands causing the shift to a higher frequency. Such a substantial increase in chemical shift is not uncommon as these large shifts have also been observed in a 6-coordinate tris(tropolonato)aluminum(III)[20] and 4-coordinate high-alumina cements.[21]

As illustrated in Fig. 1 and S1b,† the two glycolate chelators constitute the pyramidal base with a monobasic methanolate occupying the fifth position at the apex, forming the primary BU. The pseudo-pyramidal basal plane is defined *via* the oxygen atoms of the chelating glycolates with the central Al^{3+} ions 0.34–0.38 Å above this rectangular plane. Accordingly, ^{13}C MAS NMR spectra identified two distinct regions representing the various bidentate glycolate carbons (14 crystallographic carbons) (62–68 ppm) and the methanolate carbons (5 crystallographic carbons) residing at the apex of the rectangular pyramidal $^{[5]}$Al polyhedra (Fig. 3). The ^{13}C MAS NMR spectra indicate a highly ordered crystalline structure with ^{13}C line-widths approaching ~0.5 ppm (~65 Hz). Precise assignment is difficult due to the 19 crystallographic carbons have quite similar chemical environments. We note however that two of the three methanolate carbons were found in disordered environments (Fig. S1a†) and hence we speculate these to be assigned to the higher frequency resonance (~55 ppm) while the lower frequency resonance (~54 ppm) is assigned to the ordered resonance as the area ratio is found close to 2 : 1. The glycolate carbons represent seven distinct glycolate ligands, five in an ordered arrangement and two in a position-disordered configuration. However, it is interesting that the glycolate region approximately resembles a 1 : 2 : 2 : 1 : 1 ratio with respect to one another. The absence of *J*-coupling (n.a. ^{13}C, 1.1%) with the combination of MAS and high-power ^{1}H decoupling (^{1}H $\gamma B_1/2\pi$ = 100 kHz) removes the remaining chemical shielding and dipolar anisotropies, leaving behind pure isotropic chemical shift information. Without further symmetry constraints available, the exact assignment is not currently attainable.

The assembly process of the crystal structure of the aluminate complex from a 1D chain to a 2D plane and to a 3D architecture is sequentially illustrated in Fig. 4. Fig. 4a shows the 1D chain building block comprising 3 AUs that are held together by two coordinatively saturated 6-coordinate Na^+ cations with respect to oxygens, forming the in-plane Na–O ionic bonds.

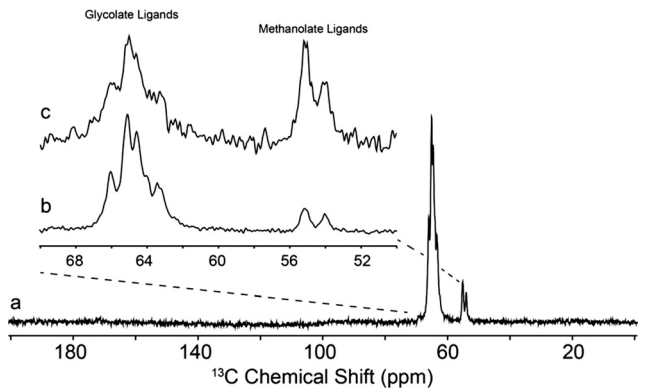

Fig. 3 ^{13}C MAS NMR spectrum of the Al complex acquired using ^{13}C{^{1}H} cross-polarization (CP) at 11.7 T (a). The inset represents a magnified region (50–70 ppm) with the glycolate and methanolate ligands identified using CP (b) and direct (Bloch) detection (c) over 8 and 60 h, respectively.

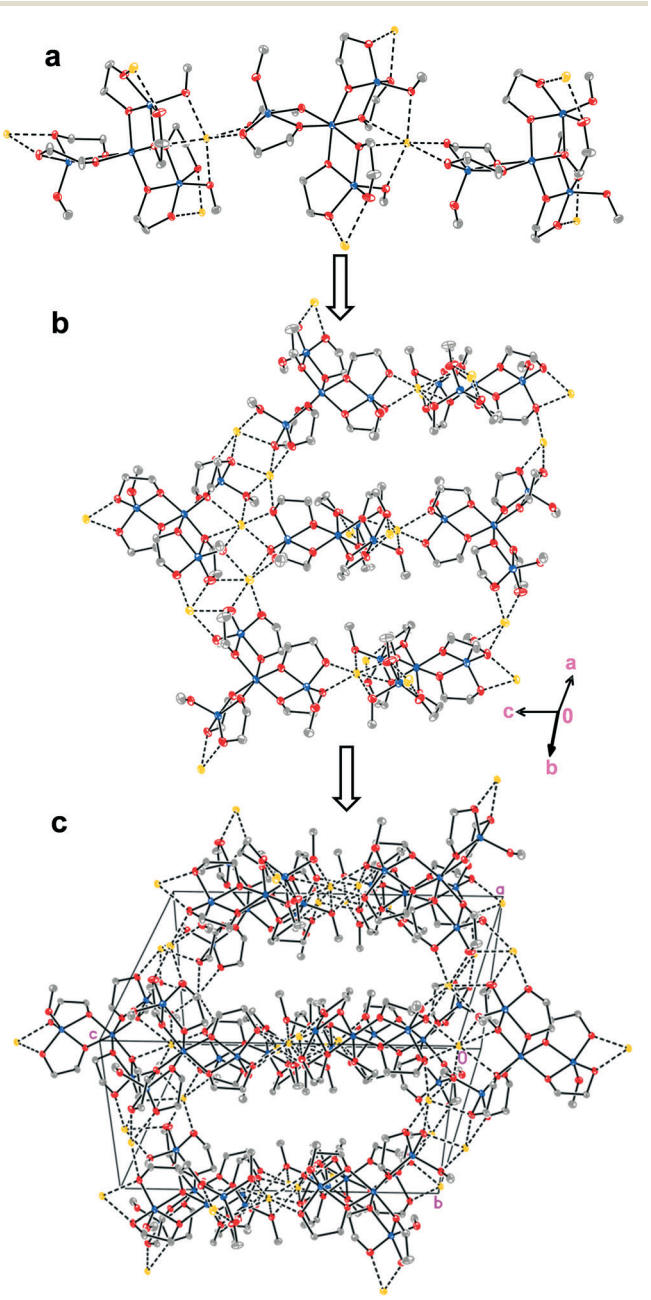

Fig. 4 Flowchart of the assembly process of the crystal structure from a 1D chain along the *c* axis (a) to a 2D plane viewed parallel to the (110) plane (b) and to a 3D architecture viewed along the [110] axis highlighting the layered structure (c). Hydrogen atoms are omitted for clarity. Blue: Al; red: O; gray: C; and yellow: Na.

To completely establish the coordinatively saturated structure, a fraction of under-coordinated 2-coordinate Na^+ species on each AU functions as a cross-linker to bind the adjacent chains together by out-of-plane Na–O ionic interactions into one 2D layer parallel to the (110) crystal plane (Fig. 4b). As shown in Fig. 4c and S2† both highlighting a layered structure, the 3D structure viewed along the crystallographic [110] axis is constructed by periodically stacking two (110) planes layer-by-layer with the interlayers cross-linked by the out-of-plane coordinatively unsaturated Na–O ionic bonds remaining on the (110) planes. Likewise, the ($\bar{1}$10)-parallel interlayers are also bound together by different out-of-plane Na^+ cations (Fig. 4c).

The experimental PXRD pattern of this sample closely matches the simulated XRD pattern derived from the SCXRD structure, suggesting the high phase purity of our powdered sample (Fig. 5). The experimental PXRD pattern exhibits a predominantly intense (110) reflection at 10.5° 2θ (8.42 Å in a (110) interplanar *d*-spacing) without any noticeable background intensity, characteristic of a (110)-dominant and well-crystallized Al complex. The typical (110) basal series peak until (220) manifests a material of a well-organized layered structure. As indicated in Fig. S2 and S3,† the orientation of the chosen parallel layers is consistent with the PXRD-characterized result. It is worth noting here that we select (110) as the basal plane of these layers instead of ($\bar{1}$10). Also, the interlayer spacing of this material could be finely tuned either by delamination or by substituting out-of-plane Na^+ cations through post ion-exchange or direct synthetic means, thus making it a potential adsorbent.

The thermal stability of the Al complex was evaluated by TGA operating in both flowing N_2 and air streams, as shown in Fig. 6. Under a flowing N_2 atmosphere, between 25 and 350 °C, there was a *ca.* 2.3% weight loss likely corresponding to the evaporation of physisorbed water, occluded MeOH solvent, and/or loosely bound methanolate-like ligands. With increasing temperature, two distinguishable weight losses were observed before the final plateau based on the DTG profile. The first very small weight loss centered at *ca.* 380 °C (~1.2%) is likely due to the loss of a small portion of relatively strongly bound methanolate-like ligands. A dramatic weight loss associated with the framework collapse was then observed between 405 and 550 °C with a temperature inflection point at 438 °C. In contrast, under flowing air, the onset degradation temperature occurred at 300 °C, and an overall weight loss of 52.9% was observed, ultimately leading to the whitened decomposition powders. The theoretical weight loss for the conversion from $C_{15}H_{33}Al_4Na_3O_{15}{\cdot}0.1CH_4O$ to a stoichiometric oxide $3NaAlO_2{\cdot}0.5Al_2O_3$ is 53.1%, which agrees well with the total weight loss occurring in the air stream, but differs from that of 46.2% in the N_2 stream. The reason for this discrepancy is the concomitant formation of minor carbon residues (~6.5%) under anaerobic conditions, as indicated by the blackened appearance of the end powders. As such, this layered material is quite thermally stable under an N_2 or air atmosphere. On the other hand, part of the in-plane Na^+ counterions and framework Al^{3+} ions are roughly sandwiched by alkoxides (Fig. 4c), thereby inhibiting to some extent the hydrolysis of Al^{3+} ions upon contact with moisture in favor of its hydrolytic stability accordingly.

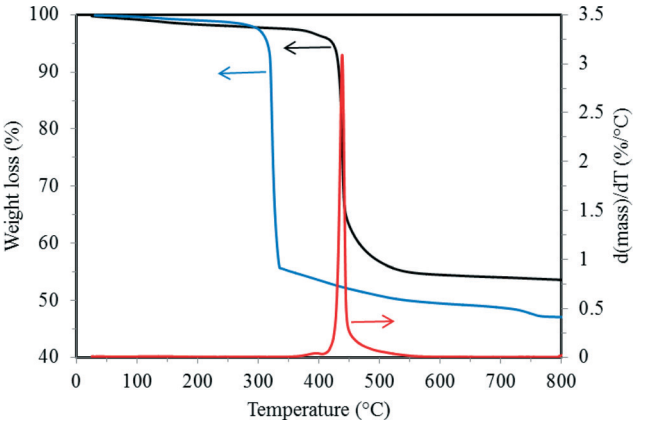

Fig. 6 TGA profiles of the Al complex in flowing N_2 (black curve) and air streams (blue curve). The red curve represents the DTG (derivative thermogravimetry) for the black trace.

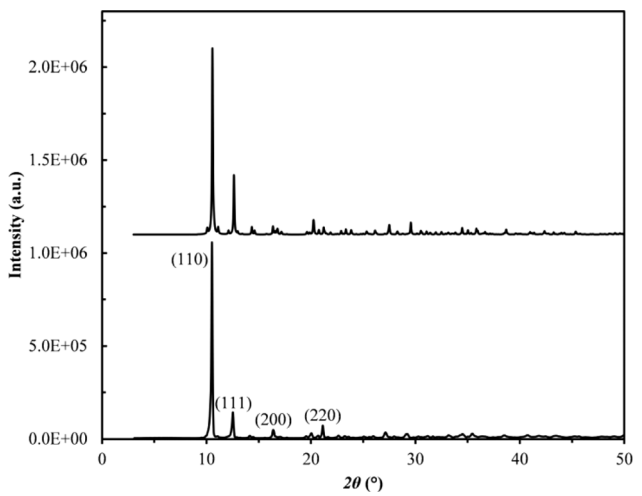

Fig. 5 Top: Simulated PXRD pattern of the as-synthesized layered sodium aluminoalcoholate single crystal. Bottom: Experimental PXRD pattern of the same powders. Well-ordered and typical 110 basal series peaks from (110) to (220) in both patterns.

Fig. 7 showed the ATR-FTIR spectrum of the Al complex. A very weak broad O–H band in the region of 3500–3200 cm^{-1} is marginally visible, indicating very low content of free alcohol or non-fully-condensed hydroxyl residues present in the crystals, and consequently very weak hydrogen bonding interaction arises. This result is in good agreement with the SCXRD and TGA analyses. The strong band at 2950–2850 cm^{-1} is due to the alkyl C–H stretching vibrations. By analogy with zeolites, the vibrational frequencies of the zeolite lattice, which result from the stretching and bending modes of the T–O units, are observed in the range between 200 and 1500 cm^{-1}.[22] Since the average Al–O bond length in zeolites is shorter than those in the current Al complex (*vide supra*),

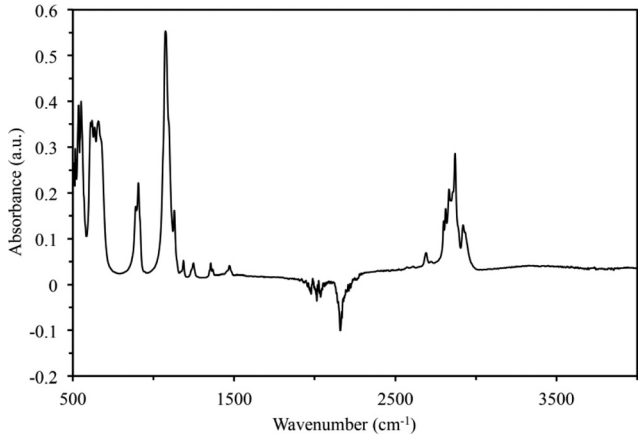

Fig. 7 ATR-FTIR spectrum of the Al complex recorded under ambient conditions.

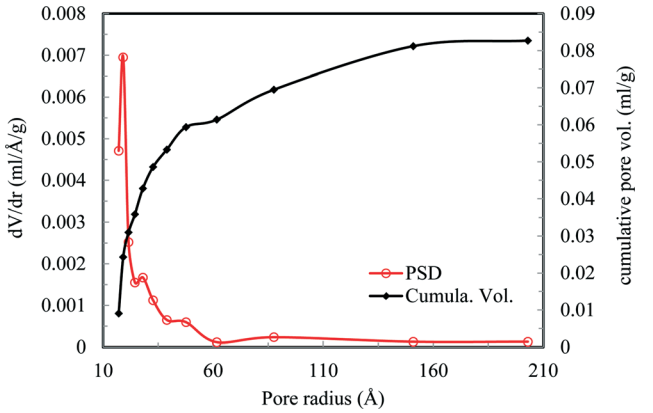

Fig. 9 PSD and cumulative pore volume of the pyrolyzed Al complex without any aqueous rinse post treatment.

the Al–O vibrational frequencies in the former shift to slightly higher wavenumbers than the latter. Hence, we attribute the absorption band at 500–1460 cm^{-1} to the Al–O vibrational frequencies of the Al complex. Obviously, no free hydroxyl groups present in its empirical formula other than those from the occluded MeOH solvent (*ca.* 10% occupancy, *cf.* Fig. S1a†) account for the fewer hydrogen bonding interactions in the crystal lattice, as confirmed by ATR-FTIR. Therefore, it justifies the effectiveness of the sodium methoxide catalyst in full condensation.

In addition, the preliminary findings suggest that this Al complex is a useful precursor towards the facile preparation of high-surface-area alumina powders by a fast pyrolysis technique (10 °C min^{-1}), giving hierarchically porous alumina grains. Fig. 8 and 9 show the N_2 sorption isotherms, and the PSD and cumulative pore volume of the pyrolyzed Al complex precursor without any aqueous leaching, respectively. It is found that the S_{BET} is up to 91.7 m^2 g^{-1} together with the V_t of 0.103 ml g^{-1} for pores smaller than 41.8 nm (width) at an RP of 0.95. After experiencing aqueous leaching of the $NaAlO_2$ component, the S_{BET} of the resulting alumina powders is slightly enhanced to 104.9 m^2 g^{-1} with the corresponding V_t nearly unchanged (not shown here). Moreover, the V_{meso} of the unwashed sample dominates the total pore volume accounting for 86.4%. As shown in Fig. 9, the mesopore radius at the maximal PSD is 19.15 Å.

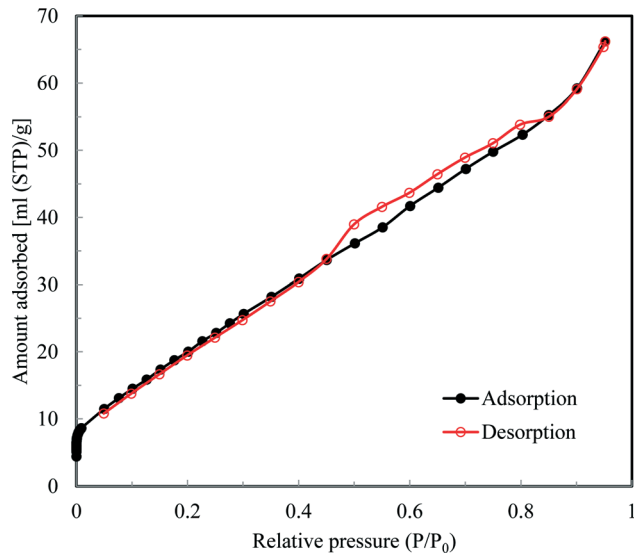

Fig. 8 N_2 adsorption/desorption isotherms of the pyrolyzed Al complex without any aqueous rinse post treatment.

Conclusions

In summary, a new well-crystallized and phase-pure tetranuclear Al complex was successfully synthesized by utilizing a modified transesterification reaction. Its layered crystal architecture comprising a network of a combination of $^{[5]}$Al and $^{[6]}$Al geometries was determined *via* SCXRD analysis and further corroborated *via* ^{27}Al and ^{13}C MAS NMR spectroscopy. Another feature is that the Al–O–Al linkage is allowed in its crystal structure as a result of slightly weakened electrostatic repulsive interactions between Al centers as compared with synthetic zeolites. The coordinatively unsaturated Al bonding sites within the porous lattice and its high thermal stability could be an attractive property for the potential applications of this material as an adsorbent. In addition, the versatile synthetic methodology proposed in this study is expected to open up a new avenue to elegantly design new porous metal–organic materials. Finally, this study provides a new route for the efficient fabrication of highly nanoporous alumina powders with hierarchical micro-/meso-porosity.

Experimental section

1. Solvothermal synthesis

A transesterification synthetic strategy was formulated to prepare this layered Al complex $Na_3[Al_4(OCH_3)_3(OCH_2CH_2O)_6]$. No special care was taken to exclude the exposure to extraneous moisture, and all manipulations were carried out in a well-ventilated fume hood. All chemicals were purchased from Sigma-Aldrich and used as received.

A recipe for $Al(OC_2H_5)_3$:3EG:$NaOCH_3$:15CH_3OH on a molar basis was originally developed. In the synthesis, 2.93 g of sodium methoxide powders (97%) were completely dissolved in 23.57 g of anhydrous methanol solvent (99.8%) under stirring before the addition of 8.79 g of aluminium ethoxide powders (97%). When the dissolution of the Al source was complete, 9.90 g of EG was rapidly added dropwise under intense agitation. The aging was maintained overnight at room temperature (RT) under stirring in a tightly sealed autoclave to ensure adequate homogenization. The solvothermal synthesis was then statically carried out at 181 °C under autogenous pressure for 5 days. The solid fraction was recovered *via* vacuum suction filtration and successively rinsed with anhydrous methanol, anhydrous tetrahydrofuran (THF, 99.9%), and further anhydrous methanol. The collected solid was vacuum dried at 80 °C for 10 h yielding 3.5 g of dry powders which were stored in a desiccator for future structural characterization. The colourless crystalline product appeared as polycrystalline powders with a few sparse X-ray-quality single crystals (*e.g.*, 0.11 × 0.04 × 0.01 mm^3 in dimension). It is worth noting that the above synthetic protocol was not optimized as the approach proposed here is robust and readily reproducible.

2. Pyrolytic preparation of porous alumina powders

To achieve a porous alumina composite for N_2 sorption measurements, fast pyrolysis was conducted on the Al complex precursor (several tens of mg) in a flowing air atmosphere (~25 ml min^{-1}) in a TGA furnace using a ramping rate of 10 °C min^{-1} up to 900 °C and a soaking duration of 3 min. Part of the pyrolyzed white powders was subsequently subjected to adequate aqueous rinse overnight at room temperature under stirring to yield pure alumina products.

3. Single-crystal X-ray diffraction (SCXRD)

Low-temperature (−173 °C) XRD data comprising φ- and ω-scans were collected using a Bruker-AXS X8 Kappa Duo diffractometer coupled with a Smart Apex II CCD detector with an IμS source of Mo K_α radiation (λ = 0.71073 Å). The structure was solved by direct methods using SHELXS[23] and refined against F^2 on all data by full-matrix least squares with SHELXL-97[24] using established refinement strategies.[25] All non-hydrogen atoms were refined anisotropically. The positions of all hydrogen atoms were calculated geometrically and refined using a riding model. The isotropic displacement parameters of all hydrogen atoms were fixed to be 1.2 times the U_{eq} value of the atom to which they are bound (1.5 for methyl groups). The representations of the positional disorders of some atoms and the asymmetric unit of the title crystal showing the empirical formula $C_{15}H_{33}Al_4Na_3O_{15}$·0.1$CH_4O$ involving ~10% occupancy of MeOH solvent molecule are illustrated in Fig. S1a.†

4. Solid-state NMR (ssNMR)

Solid-state NMR experiments were performed at either 11.7 (500 MHz, ^{1}H) or 16.4 T (697 MHz, ^{1}H) using a home-built NMR spectrometer (courtesy of Dr. D. Ruben, FBML-MIT) and a 3.2 mm Chemagnetics triple-resonance MAS probe. The crystalline sample was ground using an agate mortar and pestle under a dry atmosphere and packed quickly into a 3.2 mm (o.d.) ZrO_2 rotor (~26 μl sample). ^{27}Al spectra were acquired at a spinning frequency of $\omega_r/2\pi$ = 16 000(4) Hz and between 4096 and 65 536 co-added transients. Recycle delays were optimized using a saturation recovery experiment and set to 1.2 s using a Bloch[26] experiment with a short quantitative tip angle (14°) and to 3.0 s using a Hahn echo[27] sequence (^{27}Al $\gamma B_1/2\pi$ = 60 kHz). Non-spinning experiments (not shown here) were also collected using identical parameters above (Hahn-echo) with 83 kHz of ^{1}H continuous-wave decoupling. ^{27}Al spectra were referenced relative to 1.1 M $Al(NO_3)_3$ solution at 0 ppm.[28] ^{13}C{^{1}H} CP[29] and direct detection spectra were acquired at $\omega_r/2\pi$ = 13 450(1) Hz, 8192 co-added transients and recycle delay of 3 and 25 s, respectively. The contact time during the CP experiment was set to 1.5 ms. Both experiments were acquired using high-power (^{1}H $\gamma B_1/2\pi$ = 100 kHz) two-pulse phase modulation (TPPM)[30] ^{1}H decoupling during acquisition. ^{13}C spectra were referenced using solid adamantane to 40.49 ppm.[31] The magic angle within the probe was set using the ^{79}Br resonance of solid KBr and shimmed using adamantane prior to signal acquisition. The sample temperature was regulated between 22 and 26 °C during acquisition. All spectra were processed using RNMRP data processing software; quadrupolar line shapes were simulated using either WSOLIDS or SPINEVOLUTION software package.[32]

5. Powder X-ray diffraction (PXRD)

PXRD pattern was taken using a PANalytical X'Pert Pro Multipurpose Diffractometer in reflectance Bragg–Brentano geometry at 45 kV and 40 mA using Ni-filtered Cu Kα radiation (λ = 1.54 Å). The data collection was carried out at a constant temperature of 25 °C with a step increment of 0.084° 2θ, a counting time of 6.4 s per step, and the 2θ angular range from 3 to 50°.

6. Thermogravimetric analysis (TGA)

The sample with an initial mass of 18.48 mg was heated in a Pt pyrolytic pan at a constant ramping rate of 10 °C min^{-1} from ambient temperature up to 800 °C on a Discovery TG analyzer (TA Instruments) in flowing N_2 and air atmospheres both set to 25 ml min^{-1}. The isothermal duration at 800 °C was set to 3 min.

7. Attenuated total reflectance-Fourier transform infrared spectroscopy (ATR-FTIR)

IR absorbance spectrum was collected on the Al complex using a Nexus 870 FT-IR E.S.P. spectrometer (Thermo Scientific) equipped with an ATR accessory with a single reflection diamond crystal. The FT-IR chamber was flushed constantly with flowing N_2 stream (*ca.* 0.71 m^3 h^{-1}). Scans at a spectral resolution of ±4 cm^{-1} were taken at RT on a self-supporting sample disc

from 4000 to 500 cm^{-1}. Sixteen scans were averaged, and the resulting spectrum was background subtracted.

8. Gas sorption analysis on the pyrolyzed Al complexes with and without aqueous rinse

Gas sorption studies were carried out to investigate the textural properties of the pyrolyzed products ($3NaAlO_2 \cdot 0.5Al_2O_3$) with and without aqueous rinse. The N_2 sorption measurements were performed at −196 °C using an Autosorb iQ_2 automated gas sorption analyzer (Quantachrome). Before adsorption run, the sample was degassed under vacuum (*ca.* 0.2 Pa) at 370 °C for 12 h. Afterwards, a proper glass rod filler was inserted in a sample cell to minimize the cell dead voids. The BET (Brunauer, Emmett, and Teller) surface area (S_{BET}) was obtained by applying the BET equation to a relative pressure (RP) range of 0.05–0.30 on the adsorption branch. The total pore volume (V_t) was evaluated from the adsorbed N_2 amount at a maximum RP of 0.95. The pore size distribution (PSD) was calculated by the BJH (Barrett, Joyner, and Halenda) method on the desorption branch. The micropore volume (V_{micro}) was determined by applying the D–R (Dubinin–Radushkevich) equation to an RP range of 0.00005–0.009 on the adsorption isotherm.

Acknowledgements

This research was supported by the U.S. Department of Energy's Advanced Research Projects Agency-Energy (ARPA-E) under control no. 0471-1627. NMR studies were supported by the National Institute of Health through grants EB-001960 and EB-002026 (R.G.G.). The diffractometer was purchased with the funding from the National Science Foundation under grant no. CHE-0946721. V.K.M. is grateful to the Natural Sciences and Engineering Research Council of Canada for a postdoctoral fellowship.

References

1 G. G. Amatucci, J. M. Tarascon and L. C. Klein, *J. Electrochem. Soc.*, 1996, **143**, 1114–1123.
2 Z. Xu, J. Fan, S. Zheng, F. Ma and D. Yin, *J. Environ. Qual.*, 2009, **38**, 1302–1310.
3 N. Barrabes, D. Cornado, K. Föttinger, A. Dafinov, J. Llorca, F. Medina and G. Rupprechter, *J. Catal.*, 2009, **263**, 239–246.
4 B. Ballarin, M. Berrettoni, I. Carpani, E. Scavetta and D. Tonelli, *Anal. Chim. Acta*, 2005, **538**, 219–224.
5 R. Ma, Y. Bando and T. Sasaki, *J. Phys. Chem. B*, 2004, **108**, 2115–2119.
6 Y. Hudiono, S. Choi, S. Shu, W. J. Koros, M. Tsapatsis and S. Nair, *Microporous Mesoporous Mater.*, 2009, **118**, 427–434.
7 D. M. Bibby and M. P. Dale, *Nature*, 1985, **317**, 157–158.
8 (*a*) R. M. Laine, K. Y. Blohowiak, T. R. Robinson, M. L. Hoppe, P. Nardi, K. Kampf and J. Uhm, *Nature*, 1991, **353**, 642–644; (*b*) S. D. Kinrade, J. W. D. Nin, A. S. Schach, T. A. Sloan, K. L. Wilson and C. T. G. Knight, *Science*, 1999, **285**, 1542–1545; (*c*) B. Herreros, S. W. Carr and J. Klinowski, *Science*, 1994, **263**, 1585–1587; (*d*) K. Y. Blohowiak, D. R. Treadwell, B. L. Mueller, M. L. Hoppe, S. Jouppi, P. Kansal, K. W. Chew, C. L. S. Scotto, F. Babonneau, J. Kampf and R. M. Laine, *Chem. Mater.*, 1994, **6**, 2177–2192; (*e*) A. R. Bassindale, M. Sohail, P. G. Taylor, A. A. Korlyukov and D. E. Arkhipov, *Chem. Commun.*, 2010, **46**, 3274–3276; (*f*) C. Kobelt, C. Burschka, R. Bertermann, C. F. Guerra, F. M. Bickelhaupt and R. Tacke, *Dalton Trans.*, 2012, **41**, 2148–2162.
9 (*a*) M. C. Cruickshank and L. S. D. Glasser, *J. Chem. Soc., Chem. Commun.*, 1985, 84–85; (*b*) M. C. Cruickshank and L. S. D. Glasser, *Acta Crystallogr., Sect. C: Cryst. Struct. Commun.*, 1985, **41**, 1014–1017; (*c*) L. B. Alemany and G. W. Kirker, *J. Am. Chem. Soc.*, 1986, **108**, 6158–6162; (*d*) G. J. Gainsford, T. Kemmitt and N. B. Milestone, *Inorg. Chem.*, 1995, **34**, 5244–5251.
10 K. J. D. Mackenzie and M. E. Smith, in *Multinuclear Solid-State NMR of Inorganic Materials*, ed. R. W. Cahn, Pergamon, Oxford, 2002, vol. 6, pp. 271–324.
11 (*a*) J. A. Francis, S. G. Bott and A. R. Barron, *J. Organomet. Chem.*, 2000, **597**, 29–37; (*b*) J. Pauls and B. Neumüller, *Z. Anorg. Allg. Chem.*, 2000, **626**, 270–279; (*c*) H. Nöth, A. Schlegel and Max Suter, *J. Organomet. Chem.*, 2001, **621**, 231–241; (*d*) T.-C. Liao, Y.-L. Huang, B.-H. Huang and C.-C. Lin, *Macromol. Chem. Phys.*, 2003, **204**, 885–892; (*e*) W. Ziemkowska, S. Kucharski, A. Kolodziej and R. Anulewicz-Ostrowska, *J. Organomet. Chem.*, 2004, **689**, 2930–2939; (*f*) J. Pauls, E. Iravani, P. Köhl and B. Neumüller, *Z. Anorg. Allg. Chem.*, 2004, **630**, 876–884; (*g*) Z. Janas, L. B. Jerzykiewicz, P. Sobota, K. Szczegot and D. Wicœniewska, *Organometallics*, 2005, **24**, 3987–3994; (*h*) L. Dostál, R. Jambor, I. Císařová, J. Merna and J. Holeček, *Appl. Organomet. Chem.*, 2007, **21**, 688–693.
12 M. J. Hampden-Smith, D. S. Williams and A. L. Rheingold, *Inorg. Chem.*, 1990, **29**, 4076–4081.
13 J. Romanski, P. Nowak, K. Kosinski and J. Jurczak, *Tetrahedron Lett.*, 2012, **53**, 5287–5289.
14 M. L. Hoppe, R. M. Laine, J. Kampf, M. S. Gordon and L. W. Burggraf, *Angew. Chem., Int. Ed. Engl.*, 1993, **32**, 287–289.
15 R. W. Joyner, A. D. Smith, M. Stockenhuber and M. W. E. Van Den Berg, *Stud. Surf. Sci. Catal.*, 2004, **154**, 1406–1410.
16 W. Loewenstein, *Am. Mineral.*, 1954, **39**, 92–96.
17 X. Cheng, P. Zhao and J. F. Stebbins, *Am. Mineral.*, 2000, **85**, 1030–1037.
18 J. F. Stebbins, P. Zhao, S. K. Lee and X. Cheng, *Am. Mineral.*, 1999, **84**, 1680–1684.
19 J. Klinowski, S. W. Carr, S. E. Tarling and P. Barnes, *Nature*, 1987, **330**, 56–58.
20 R. W. Schurko, R. E. Wasylishen and H. Foerster, *J. Phys. Chem. A*, 1998, **102**, 9750–9760.
21 J. Skibsted, E. Henderson and H. J. Jakobsen, *Inorg. Chem.*, 1993, **32**, 1013–1027.
22 A. Jentys and J. A. Lercher, *Stud. Surf. Sci. Catal.*, 2001, **137**, 345–386.

23 G. M. Sheldrick, *Acta Crystallogr., Sect. A: Found. Crystallogr.*, 1990, **46**, 467–473.
24 G. M. Sheldrick, *Acta Crystallogr., Sect. A: Found. Crystallogr.*, 2008, **64**, 112–122.
25 P. Müller, *Crystallogr. Rev.*, 2009, **15**, 57–83.
26 F. Bloch, *Phys. Rev.*, 1946, **70**, 460–474.
27 E. L. Hahn, *Phys. Rev.*, 1950, **80**, 580–594.
28 R. K. Harris and E. D. Becker, *J. Magn. Reson.*, 2002, **156**, 323–326.
29 A. Pines, J. S. Waugh and M. G. Gibby, *J. Chem. Phys.*, 1972, **56**, 1776–1777.
30 A. E. Bennett, C. M. Rienstra, M. Auger, K. V. Lakshmi and R. G. Griffin, *J. Chem. Phys.*, 1995, **103**, 6951–6958.
31 C. R. Morcombe and K. W. Zilm, *J. Magn. Reson.*, 2003, **162**, 479–486.
32 (*a*) K. Eichele, *WSolids1-Solid State NMR Simulations*, Version 1.20.21, Universität Tübingen, 2013; (*b*) M. Veshtort and R. G. Griffin, *J. Magn. Reson.*, 2006, **178**, 248–282.

